Acta Crystallographica Section F
Structural Biology and Crystallization Communications
ISSN 1744-3091

Cocrystal structure of the ICAP1 PTB domain in complex with a KRIT1 peptide

Weizhi Liu[a,b]* and Titus J. Boggon[a,c]*

[a]Department of Pharmacology, Yale University School of Medicine, 333 Cedar Street, New Haven, CT 06520, USA, [b]College of Marine Life Sciences, Ocean University of China, 5 Yushan Road, Qingdao 266003, People's Republic of China, and [c]Yale Cancer Center, Yale University School of Medicine, 333 Cedar Street, New Haven, CT 06520, USA

Correspondence e-mail: liuweizhi@ouc.edu.cn, titus.boggon@yale.edu

Received 21 March 2013
Accepted 19 April 2013

PDB Reference: ICAP1–KRIT1$^{170–198}$, 4jif

Integrin cytoplasmic domain-associated protein-1 (ICAP1) is a suppressor of integrin activation and directly binds to the cytoplasmic tail of β1 integrins; its binding suppresses integrin activation by competition with talin. Krev/Rap1 interaction trapped-1 (KRIT1) releases ICAP1 suppression of integrin activation by sequestering ICAP1 away from integrin cytoplasmic tails. Here, the cocrystal structure of the PTB domain of ICAP1 in complex with a 29-amino-acid fragment (residues 170–198) of KRIT1 is presented to 1.7 Å resolution [the resolution at which $\langle I/\sigma(I)\rangle = 2.9$ was 1.83 Å]. In previous studies, the structure of ICAP1 with integrin β1 was determined to 3.0 Å resolution and that of ICAP1 with the N-terminal portion of KRIT1 (residues 1–198) was determined to 2.54 Å resolution; therefore, this study provides the highest resolution structure yet of ICAP1 and allows further detailed analysis of the interaction of ICAP1 with its minimal binding region in KRIT1.

1. Introduction

Integrin cytoplasmic domain-associated protein-1 (ICAP1) is a 200-residue cytoplasmic protein with a PTB domain at its C-terminus. This protein is a negative regulator of integrin adhesion receptors (Chang *et al.*, 1997, 2002), and through its interaction with a β1 integrin NP*X*Y motif ICAP1 has been found to play important roles in many critical physiological and pathological processes, including cell proliferation (Fournier *et al.*, 2005; Calderwood *et al.*, 2003), angiogenesis (Brütsch *et al.*, 2010) and bone development (Bouvard *et al.*, 2007; Brunner *et al.*, 2011). ICAP1 has also been discovered to be able to interact with an NP*X*Y motif in the protein KRIT1 (Krev/Rap1 interaction trapped-1, also known as cerebral cavernous malformations 1; CCM1), the product of the *CCM1* gene. *CCM1* is one of three genes associated with the familial form of the disease cerebral cavernous malformations (CCM; Cavalcanti *et al.*, 2012), and crystal structures of KRIT1 have recently been determined (Li *et al.*, 2012; Liu *et al.*, 2013; Gingras *et al.*, 2012). Loss of KRIT1 results in the acquisition of mulberry-shaped neurovascular lesions containing thin-walled capillary channels with single endothelial layers and leaky endothelial cell junctions. CCM predisposes to severe outcomes including stroke, epilepsy and neurological disorders (Cavalcanti *et al.*, 2012).

Recently, we elucidated the molecular mechanism of how KRIT1 antagonizes ICAP1-mediated modulation of integrin activation (Liu *et al.*, 2013). We showed that ICAP1 could specifically bind to integrin β1 *via* a canonical PTB–NP*X*Y binding interface, but that ICAP1 binds to KRIT1 through both a canonical PTB–NP*X*Y binding interface and an addition site that we termed the 'RR' site. Our previous studies determined the cocrystal structures of ICAP1 with an integrin β1 peptide to 3.0 Å resolution and of ICAP1 with a KRIT1 N-terminal region (residues 1–198) to 2.54 Å resolution (Liu *et al.*, 2013). Therefore, the best resolution for an ICAP1 structure is currently 2.54 Å. On analysis of our cocrystal structure of ICAP1 with KRIT1 we discovered that the N-terminal portion contains a Nudix-fold domain, so for the present study we wondered whether exclusion of the Nudix domain would allow both co-expression and cocrystallization of a short portion of KRIT1 with ICAP1. Analysis of our

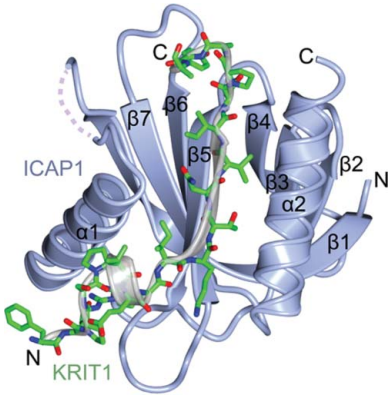

© 2013 International Union of Crystallography
All rights reserved

previous structure suggested that a short KRIT1 region (residues 170–198) is sufficient to bind ICAP1; therefore, in the current study we co-expressed, copurified and cocrystallized KRIT1$^{170–198}$ (KRIT1 residues 170–198) with the ICAP1 PTB domain (ICAP1 residues 49–200). We obtained a high-resolution (1.7 Å) structure of the ICAP1–KRIT$^{170–198}$ complex crystal structure, which not only validates the previous observation of ICAP1–KRIT1 interaction but also facilitates future studies of complexes of ICAP1 with other binding partners.

2. Materials and methods

2.1. Cloning, co-expression and copurification of ICAP1–KRIT$^{170–198}$

Codon-optimized human ICAP1 (residues 49–200; GenScript) in a modified pET-32 vector with an N-terminal hexahistidine (6×His) tag was co-transformed into *Escherichia coli* BL21(DE3) with KRIT1 (residues 170–198) in a pGEX-6p-1 (GE) vector with an N-terminal glutathione *S*-transferase (GST) tag. For co-expression of the protein complex, the cells were induced at an OD_{600} of 0.6 by 0.2 m*M* IPTG at 291 K overnight. After harvesting, the cells were lysed using a freeze–thaw protocol and sonication with 1 mg ml^{-1} lysozyme and were clarified by centrifugation at 20 000*g*. The ICAP1–KRIT1$^{170–198}$ complex was affinity-purified using Ni Sepharose 6 Fast Flow affinity-matrix beads (GE) and was eluted using 500 m*M* imidazole in 20 m*M* Tris pH 8.0 buffer containing 500 m*M* NaCl. The eluted protein was then dialyzed at 277 K overnight against PBS buffer with tobacco etch virus (TEV) protease to remove the ICAP1 6×His tag. The complex was affinity-purified on glutathione Sepharose 4B beads (GE) and the N-terminal KRIT1$^{170–198}$ GST tag was removed with PreScission protease on the beads at 277 K overnight. Finally, the ICAP1–KRIT1$^{170–198}$ complex was further copurified on a Superdex 75 column (GE). ICAP1–KRIT1$^{170–198}$ eluted as a monodisperse peak in 20 m*M* HEPES pH 7.5, 100 m*M* NaCl, 1 m*M* DTT, 1 m*M* EDTA.

2.2. Crystallization, data collection, structure determination and refinement

The ICAP1–KRIT1$^{170–198}$ complex was concentrated to 15.0 mg ml^{-1} for crystallization trials. Initial crystallization screening was performed using the sitting-drop method and The JCSG+ and PEGs Suites crystallization screening kits (Qiagen) with a Matrix Hydra II eDrop crystallization robot (Murthy *et al.*, 2007). Initial crystals were observed overnight at room temperature in conditions consisting of 20% PEG 3350, 0.2 *M* $MgCl_2$. We then conducted detailed grid screening around these conditions by varying the $MgCl_2$ and PEG 3350 concentrations using the hanging-drop vapour-diffusion method at room temperature (298 K). The best crystals grew within 3–4 d in very similar conditions to the initial screens: 18–20% PEG 3350 with 0.2 *M* $MgCl_2$. Optimal conditions for crystal growth were achieved in a total crystallization drop size of 2 µl using a 1:1 ratio of protein to precipitant equilibrated against a precipitant well volume of 300 µl. For cryoprotection, crystals were transferred into 30% PEG 3350 with 0.2 *M* $MgCl_2$ for 1 min. 180° of data were collected on beamline X29A at the National Synchrotron Light Source (NSLS) and 120° of data were processed using *HKL*-2000 (Otwinowski & Minor, 1997). Initial structure solution was obtained by molecular replacement with *Phaser* (McCoy *et al.*, 2005) and ICAP1 (chain *B*) using the 2.54 Å resolution structure of ICAP1 with KRIT1$^{1–198}$ (PDB entry 4dx8; Liu *et al.*, 2013) as the search model. The initial solution allowed autobuilding using *ARP*/*wARP* (Cohen *et al.*, 2004), which resulted in 132 residues of ICAP1 and 17 residues of KRIT1 being built. Iterative rounds of model building and refinement with TLS were conducted, with refinement conducted using *PHENIX* (Adams *et al.*, 2002) and *REFMAC*5 (Murshudov *et al.*, 2011); model building utilized *Coot* (Emsley & Cowtan, 2004). The final structure had good geometry, with the Ramachandran statistics showing all residues in favored or allowed conformations. *MolProbity* analysis (Chen *et al.*, 2010) yielded a clashscore of 4.25 (97th percentile). Analysis of the protein interactions was performed using *PDBsum* (Laskowski, 2001), and structural figures were generated using *CCP*4*mg* (McNicholas *et al.*, 2011). Data-collection and refinement statistics are given in Table 1.

Table 1
Data-collection and refinement statistics.

Values in parentheses are for the highest resolution shell processed and those in square brackets are for that in which $\langle I/\sigma(I)\rangle$ = 2.9.

Data collection	
X-ray source	X29, NSLS
Space group	$P6_522$
Unit-cell parameters (Å, °)	$a = b = 81.0$, $c = 89.6$, $\alpha = \beta = 90$, $\gamma = 120$
Wavelength (Å)	1.0750
Resolution range (Å)	35–1.70 (1.76–1.70) [1.91–1.83]
Unique reflections	19620
Completeness (%)	99.6 (100) [99.9]
$\langle I/\sigma(I)\rangle$	23.2 (1.3) [2.9]
R_{merge} (%)	6.1 (230.9) [98.2]
$R_{p.i.m.}$† (%)	2.9 (67.6) [28.9]
Multiplicity	12.4 (12.3) [12.3]
Wilson *B* factor (Å^2)	28.3
Refinement statistics	
Resolution (Å)	32.7–1.7 (1.79–1.70)
R factor (%)	19.6 (38.6)
Free *R* factor (%)	22.6 (35.8)
Residues built	ICAP1, 60–76 + 82–194; KRIT1, 178–196
Free *R* reflections (%)	5.1 (4.8)
Free *R* reflections (No.)	1001 (126)
No. of non-H atoms	1211
No. of water molecules	116
Model quality	
R.m.s.d., bond lengths (Å)	0.007
R.m.s.d., bond angles (°)	1.07
Mean *B* factors	
Overall (Å^2)	39.98
Protein atoms (*A*/*B*) (Å^2)	39.2/41.9
Water (Å^2)	44.6
Ramachandran plot, residues in (%)	
Favored regions	99.3
Allowed regions	0.7
Disallowed regions	0

† $R_{p.i.m.}$ was calculated using *RMERGE* (M. Weiss, unpublished work).

3. Results and discussion

3.1. Expression and purification of the ICAP1–KRIT1$^{170–198}$ complex

ICAP1 is poorly soluble when expressed alone, as in the *E. coli* system. Previously, we showed that its solubility could be improved by co-expression with the N-terminal portion of KRIT1, KRIT1$^{1–198}$ (Liu *et al.*, 2013). This N-terminal portion of KRIT1 contains both the ICAP1-binding region and the KRIT1 Nudix domain (Liu *et al.*, 2013); therefore, we wondered whether co-expression of ICAP1 with the minimal binding region of KRIT1 would also allow improved solubility of ICAP1. Our previous study showed that the minimal ICAP1-binding region of KRIT1 includes residues 170–198 and binds ICAP1 with an affinity of 1.24 ± 0.03 µ*M* by surface plasmon resonance (Liu *et al.*, 2013); therefore, we tested co-expression of 6×His-tagged ICAP1$^{49–200}$ and GST-tagged KRIT1$^{170–198}$. We found that co-expression significantly improved the yield of ICAP1.

Following affinity purification of the 6×His-tagged ICAP1, we removed the 6×His tag using TEV protease and bound the complex to glutathione Sepharose beads. PreScission protease was used to remove the GST tag and allow the elution of the ICAP1–KRIT1$^{170–198}$ complex. The final step of purification was size-exclusion chromatography (Fig. 1*a*) and the complex was concentrated for crystallization (Fig. 1*b*).

3.2. Structure determination and refinement of the ICAP1–KRIT1$^{170–198}$ complex

Following concentration, ICAP1–KRIT1$^{170–198}$ cocrystals grew to 10 × 20 × 100 µm within 5 d at room temperature using the hanging-drop vapor-diffusion technique against precipitant conditions of 20% PEG 3350, 0.2 *M* $MgCl_2$ (Fig. 1*c*). Single crystals were separated from flower-like clusters (Fig. 1*c*) using a CryoLoop and the ICAP1–KRIT1$^{170–198}$ cocrystals diffracted to 1.70 Å resolution [the resolution for which $\langle I/\sigma(I)\rangle$ = 2.9 was 1.83 Å]. 180° of data were collected on beamline X29A of the National Synchrotron Light Source (NSLS) at Brookhaven National Laboratory, New York, USA. The ICAP1–KRIT1$^{170–198}$ cocrystal belonged to space group $P6_522$ and Matthews coefficient analysis (V_M = 2.2 Å^3 Da^{-1}) suggested that one ICAP1–KRIT1$^{170–198}$ complex exists in the asymmetric unit. We used a single copy of ICAP1 from our ICAP1–KRIT1$^{1–198}$ complex structure as the search model for molecular replacement using *Phaser* (McCoy *et al.*, 2005). *Phaser* yielded a rotation *Z*-score of 8.7 and a final translation *Z*-score of 37.1. Autobuilding was then utilized to mitigate phase bias using *ARP*/*wARP* (Cohen *et al.*, 2004), refinement was conducted to 1.7 Å resolution using the maximum-likelihood programs *REFMAC*5 (Murshudov *et al.*, 2011) and *PHENIX* (Adams *et al.*, 2002), and model building was conducted using *Coot* (Emsley & Cowtan, 2004). The refined model has good electron density (Fig. 1*d*) and has been deposited in the Protein Data Bank under accession code 4jif.

3.3. Structural analysis of ICAP1–KRIT1$^{170–198}$

ICAP1 is folded as a Dab-like PTB domain with seven β-strands and two α-helices (Fig. 2*a*). Comparison of the ICAP1 PTB domain with previously determined ICAP1 structures show r.m.s.d.s of 1.0 Å over 125 residues for ICAP1 in complex with integrin β1 (PDB entry 4dx9; Liu *et al.*, 2013) and of 1.0 Å over 129 residues for ICAP1 in complex with KRIT1$^{1–198}$ (PDB entry 4dx8; Liu *et al.*, 2013; Fig. 2*b*). This suggests that no significant structural changes occur in ICAP1 on binding to either KRIT1 or integrin β1. Interestingly, ICAP1 displays an r.m.s.d. of only 2.0 Å over 107 C^α atoms to a predicted ICAP1 structure (PDB entry 1k11; Chang *et al.*, 2002; Fig. 2*c*). For KRIT1$^{170–198}$, residues 178–196 are visible in the electron density (Fig. 2*a*). These display an r.m.s.d. of 0.65 Å over 17 residues when compared with the previously determined structure of ICAP1 in complex with KRIT1$^{1–198}$ (PDB entry 4dx8; Liu *et al.*, 2013).

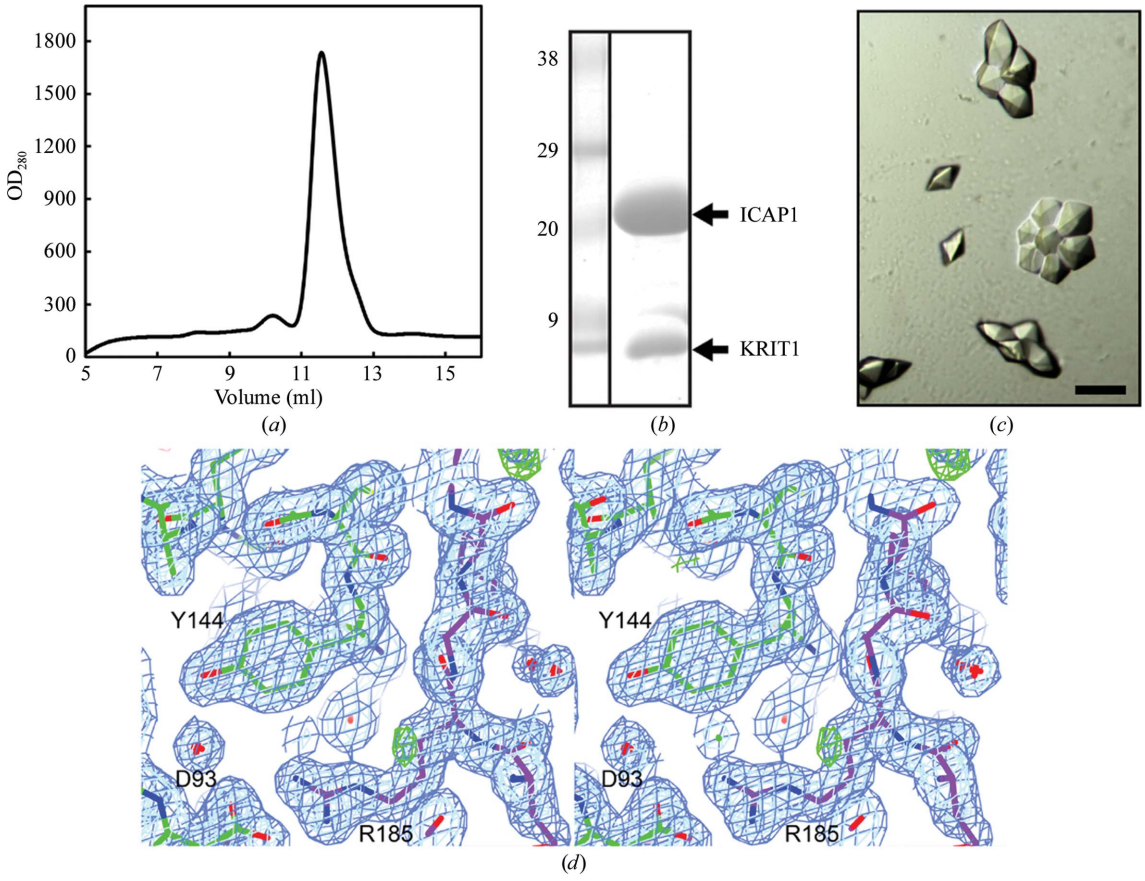

Figure 1
Protein purification and crystallization of the ICAP1–KRIT1$^{170–198}$ complex. (*a*) Gel filtration of the ICAP1–KRIT1$^{170–198}$ complex on a Superdex 75 column. The complex was eluted in 20 m*M* HEPES buffer pH 7.5 including 100 m*M* NaCl, 1 m*M* EDTA and 1 m*M* DTT. (*b*) SDS–PAGE (15%) of the ICAP1–KRIT1$^{170–198}$ complex before crystallization. (*c*) Crystals of the ICAP1–KRIT1$^{170–198}$ complex growing in conditions consisting of 20% PEG 3350, 0.2 *M* $MgCl_2$. The crystals grew as clusters resembling flowers; the petals were separated for single-crystal data collection. The black bar indicates 100 µm. (*d*) Stereoview of example electron density for the refined structure. ICAP1 is shown in green and KRIT1 is shown in purple. Residues Tyr144 and Asp93 of ICAP1 and residue Arg185 of KRIT1 are labeled. $2F_{obs} - F_{calc}$ maps are shown in dark blue (1σ) and light blue (2σ); $2F_{obs} - F_{calc}$ maps are shown in green (+3σ) and red (−3σ).

Structural analysis of ICAP1–KRIT1$^{170–198}$ using the *DALI* server (Holm & Sander, 1997) shows that the highest structural similarity of ICAP1 is to PH/PTB domains of EPS8 (PDB entries 2cy4 and 2cy5; E. Mizohata, H. Hamana, S. Morita, Y. Kinoshita, K. Nagano, H. Uda,

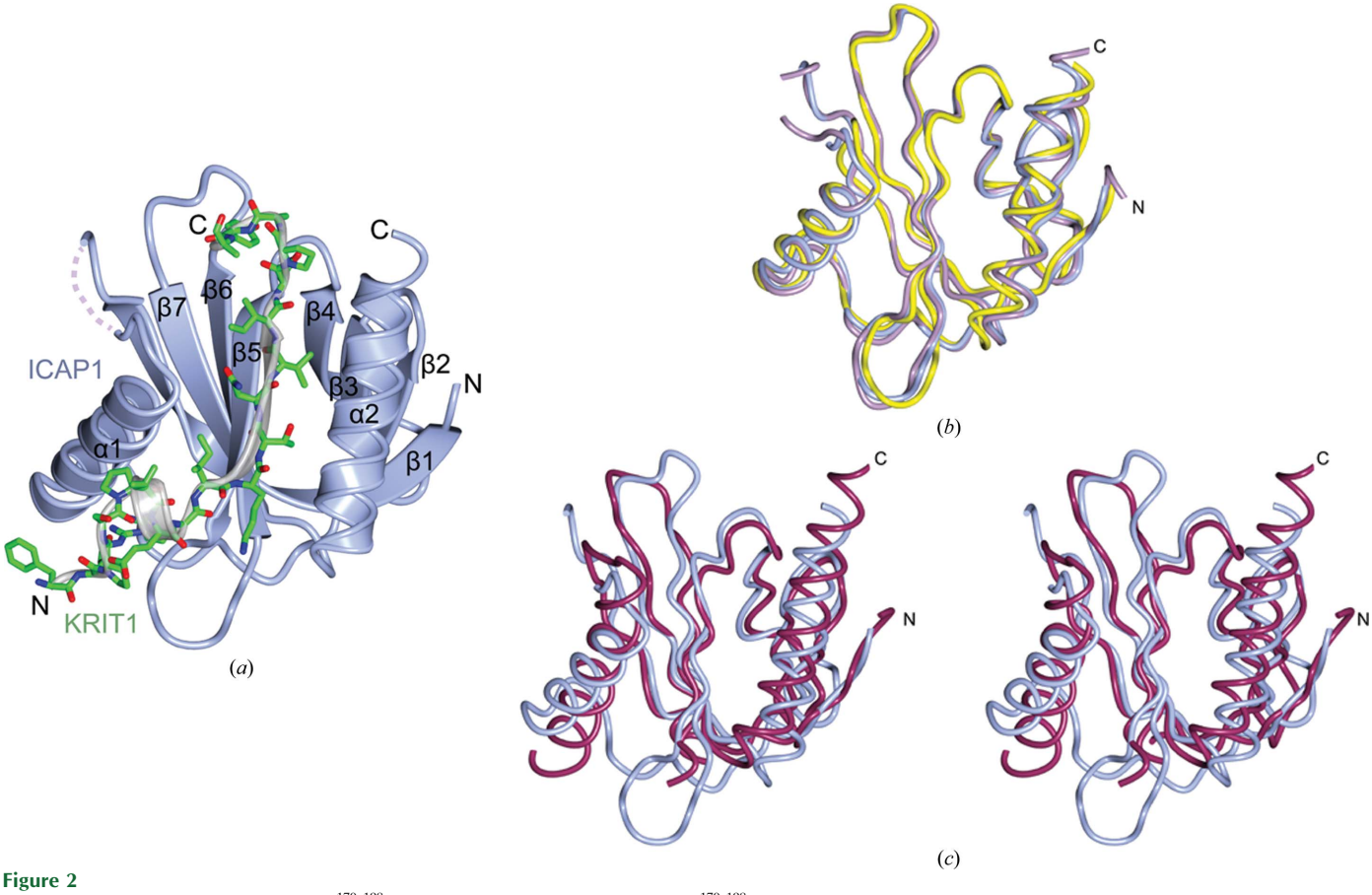

Figure 2
Cocrystal structure of ICAP1 with KRIT1$^{170–198}$. (*a*) Overall view of the ICAP1–KRIT1$^{170–198}$ complex structure. ICAP1 is shown in blue with secondary-structure elements labeled. KRIT1 is shown in cylinder format with secondary-structure elements shown in gray. (*b*) Superposition of ICAP1 crystal structures. ICAP1 in complex with KRIT1$^{170–198}$ (this structure) is colored blue. ICAP1 in complex with KRIT1 residues 1–198 (PDB entry 4dx8) is colored purple. ICAP1 in complex with integrin β1 (PDB entry 4dx9) is colored yellow. N- and C-termini are indicated. (*c*) Stereoview of the superposition of ICAP1 with the predicted structure of ICAP1. ICAP1 in complex with KRIT1$^{170–198}$ (this structure) is colored blue. The predicted structure of ICAP1 (PDB entry 1k11) is shown in purple. N- and C-termini are indicated.

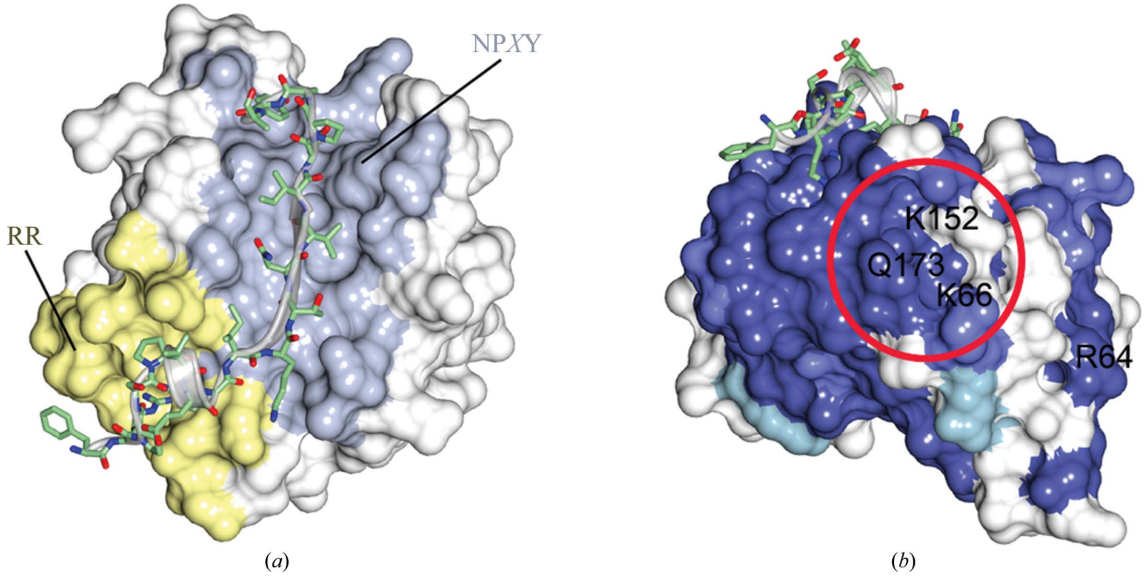

Figure 3
Analysis of ICAP1 binding surfaces. (*a*) Binding of ICAP1 and KRIT1. The surface of ICAP1 is shown with the NP*X*Y binding site shown in blue and the RR binding site shown in yellow. KRIT1 is shown in cylinder format with secondary-structure elements shown in gray. (*b*) Conservation of ICAP1 around the PH-fold phosphotidylinositol headgroup binding site (shown with a red circle). ICAP1 shows high conservation in this region. Dark blue indicates complete conservation based on alignment over 34 species (see Liu *et al.*, 2013 for alignment). Residues discussed in the text are indicated.

T. Terada, M. Shirouzu & S. Yokoyama, unpublished work) and APPL1 (PDB entry 2ela; Li *et al.*, 2007; r.m.s.d. of 2.3–2.9 Å over 114–123 residues; *DALI* *Z*-scores of 13.8–15.5).

3.4. Analysis of the interaction between ICAP1 and KRIT1

ICAP1 binds to KRIT1 by an extended bidentate interaction using two surfaces termed the NP*X*Y site and the RR site. The RR site is a novel PTB-recognition binding site (Liu *et al.*, 2013). The binding site in our new structure of ICAP1 in complex with its minimal binding region of KRIT1 confirmed these results (Fig. 3*a*), highlighting the bidentate interaction. We note, however, that there are small differences between the ICAP1–KRIT1$^{170–198}$ and the ICAP1–KRIT1$^{1–198}$ structures. In the ICAP1–KRIT1$^{1–198}$ complex structure there is a helical region formed by residues ^{172}HFIPA; however, no electron density is visible for this region in ICAP1–KRIT1$^{170–198}$, probably owing to crystal packing. Consequently, the ICAP1–KRIT1$^{170–198}$ cocrystal has a smaller buried surface area of 1925 Å^2 compared with the 2969 Å^2 buried in the ICAP1–KRIT1$^{1–198}$ complex.

3.5. Conservation analysis of ICAP1

On analysis of the surface conservation of ICAP1, we find that there is a significant region of complete conservation at the site that encompasses the region in ICAP1 that is analogous to the PH-domain phosphatidylinositol headgroup site (Fig. 3*b*). Some residues of ICAP1 that could allow phosphotidylinositol headgroup binding are completely conserved, including Arg64^{ICAP}, Lys66^{ICAP}, Gln173^{ICAP} and Lys152^{ICAP}; these correspond to the structural locations of X11 residues Lys43, Lys45, Lys142 and Arg124, respectively, raising the potential that ICAP1 could also bind phosphotidylinositol headgroups. This possibility remains to be investigated.

This study provides the highest resolution structure yet of ICAP1 and allows further detailed analysis of the interaction of ICAP1 with its minimal binding region in KRIT1.

We thank J. Hu, Y. Ha, K. M. Draheim, R. Zhang and D. A. Calderwood. Crystallographic data were collected on beamline X29 at NSLS. TJB is funded by NIH.

References

Adams, P. D., Grosse-Kunstleve, R. W., Hung, L.-W., Ioerger, T. R., McCoy, A. J., Moriarty, N. W., Read, R. J., Sacchettini, J. C., Sauter, N. K. & Terwilliger, T. C. (2002). *Acta Cryst.* D**58**, 1948–1954.
Bouvard, D., Aszodi, A., Kostka, G., Block, M. R., Albigès-Rizo, C. & Fässler, R. (2007). *Development*, **134**, 2615–2625.
Brunner, M., Millon-Frémillon, A., Chevalier, G., Nakchbandi, I. A., Mosher, D., Block, M. R., Albigès-Rizo, C. & Bouvard, D. (2011). *J. Cell Biol.* **194**, 307–322.
Brütsch, R., Liebler, S. S., Wüstehube, J., Bartol, A., Herberich, S. E., Adam, M. G., Telzerow, A., Augustin, H. G. & Fischer, A. (2010). *Circ. Res.* **107**, 592–601.
Calderwood, D. A., Fujioka, Y., de Pereda, J. M., García-Alvarez, B., Nakamoto, T., Margolis, B., McGlade, C. J., Liddington, R. C. & Ginsberg, M. H. (2003). *Proc. Natl Acad. Sci. USA*, **100**, 2272–2277.
Cavalcanti, D. D., Kalani, M. Y., Martirosyan, N. L., Eales, J., Spetzler, R. F. & Preul, M. C. (2012). *J. Neurosurg.* **116**, 122–132.
Chang, D. D., Hoang, B. Q., Liu, J. & Springer, T. A. (2002). *J. Biol. Chem.* **277**, 8140–8145.
Chang, D. D., Wong, C., Smith, H. & Liu, J. (1997). *J. Cell Biol.* **138**, 1149–1157.
Chen, V. B., Arendall, W. B., Headd, J. J., Keedy, D. A., Immormino, R. M., Kapral, G. J., Murray, L. W., Richardson, J. S. & Richardson, D. C. (2010). *Acta Cryst.* D**66**, 12–21.
Cohen, S. X., Morris, R. J., Fernandez, F. J., Ben Jelloul, M., Kakaris, M., Parthasarathy, V., Lamzin, V. S., Kleywegt, G. J. & Perrakis, A. (2004). *Acta Cryst.* D**60**, 2222–2229.
Emsley, P. & Cowtan, K. (2004). *Acta Cryst.* D**60**, 2126–2132.
Fournier, H.-N., Dupé-Manet, S., Bouvard, D., Luton, F., Degani, S., Block, M. R., Retta, S. F. & Albiges-Rizo, C. (2005). *Mol. Biol. Cell*, **16**, 1859–1871.
Gingras, A. R., Liu, J. J. & Ginsberg, M. H. (2012). *J. Cell Biol.* **199**, 39–48.
Holm, L. & Sander, C. (1997). *Nucleic Acids Res.* **25**, 231–234.
Laskowski, R. A. (2001). *Nucleic Acids Res.* **29**, 221–222.
Li, J., Mao, X., Dong, L. Q., Liu, F. & Tong, L. (2007). *Structure*, **15**, 525–533.
Li, X., Zhang, R., Draheim, K. M., Liu, W., Calderwood, D. A. & Boggon, T. J. (2012). *J. Biol. Chem.* **287**, 22317–22327.
Liu, W., Draheim, K. M., Zhang, R., Calderwood, D. A. & Boggon, T. J. (2013). *Mol. Cell*, **49**, 719–729.
McCoy, A. J., Grosse-Kunstleve, R. W., Storoni, L. C. & Read, R. J. (2005). *Acta Cryst.* D**61**, 458–464.
McNicholas, S., Potterton, E., Wilson, K. S. & Noble, M. E. M. (2011). *Acta Cryst.* D**67**, 386–394.
Murshudov, G. N., Skubák, P., Lebedev, A. A., Pannu, N. S., Steiner, R. A., Nicholls, R. A., Winn, M. D., Long, F. & Vagin, A. A. (2011). *Acta Cryst.* D**67**, 355–367.
Murthy, T., Wang, Y., Reynolds, C. & Boggon, T. (2007). *J. Assoc. Lab. Autom.* **12**, 213–218.
Otwinowski, Z. & Minor, W. (1997). *Methods Enzymol.* **276**, 307–326.